You *et al. Chem. Biol. Technol. Agric.* (2024) 11:11
https://doi.org/10.1186/s40538-024-00534-8

Chemical and Biological Technologies in Agriculture

RESEARCH

Open Access

Coproduction of bio-microbicide and silver nano-microbicide mediated by endospore-forming *Bacillus* and their synergetic control of plant disease

Yuxin You[1], Chen Wang[1], Yasmine Abdallah[1,2], Quanhong Liu[1], Chentao Liu[1], Jinyan Luo[3], Dejiang Dai[4], Salim S. Al-Rejaie[5], Mohamed Mohany[5], Bin Li[1*], Solabomi Olaitan Ogunyemi[1*] and Qianli An[1*]

Abstract

Background One-pot synthesis of metal nanoparticles under ambient temperature and pressure using reducing and stabilizing materials from microbes is energy-effective and ecofriendly, but upstream extraction of biological raw materials and downstream purification of nanoparticles from bioreactors are laborious and expensive. To simplify the productive process for using metal nanoparticles as microbicides to control plant pathogens, we use an endospore-forming *Bacillus* biocontrol agent to produce the nano-microbicide and use the bacterial raw materials as bio-microbicides together with the nano-microbicide.

Results *Bacillus* cells at the stationary phase form endospores and tolerate Ag^+ and Ag nanoparticles (AgNPs), while the cell-free culture supernatant (CFCS) mediates the synthesis of AgNPs. AgNPs produced from the *Bacillus* culture and CFCS show similar physical, chemical, and electrical characteristics, and bactericidal and anti-biofilm activities. Moreover, the diluted products effectively protect the kiwifruit leaves from the infection of the pathogen *Pseudomonas syringae* pv. *actinidiae*.

Conclusions This coproduction of bio-microbicide and nano-microbicide is a totally green one-pot synthesis process without extraction and purification and without production of waste and can be easily scaled up using the existing fermentation processing of *Bacillus* biocontrol agents. The application of the synergistic bio-microbicide and nano-microbicide can effectively control the bacterial canker disease of kiwifruit plants.

Highlights

- Endospore-forming *Bacillus* cells can tolerate metal and metal nanoparticles.
- *Bacillus* biocontrol agents can be used as bio-microbicides and to produce nano-microbicides.
- Coproduction of bio-microbicides and nano-microbicides is a solution of large-scale production of nano-microbicides.

*Correspondence:
Bin Li
libin0571@zju.edu.cn
Solabomi Olaitan Ogunyemi
0622251@zju.edu.cn
Qianli An
an@zju.edu.cn
Full list of author information is available at the end of the article

- Screening biocontrol *Bacillus* agents producing metal nanoparticle in bacterial culture is a key of this solution.
- Cooperation of bio-microbicides and nano-microbicides can effectively control the bacterial canker disease of kiwifruit.

Keywords Biocontrol, Green synthesis, Metallic nanoparticle, Nanopesticide, One-pot synthesis

Graphical Abstract

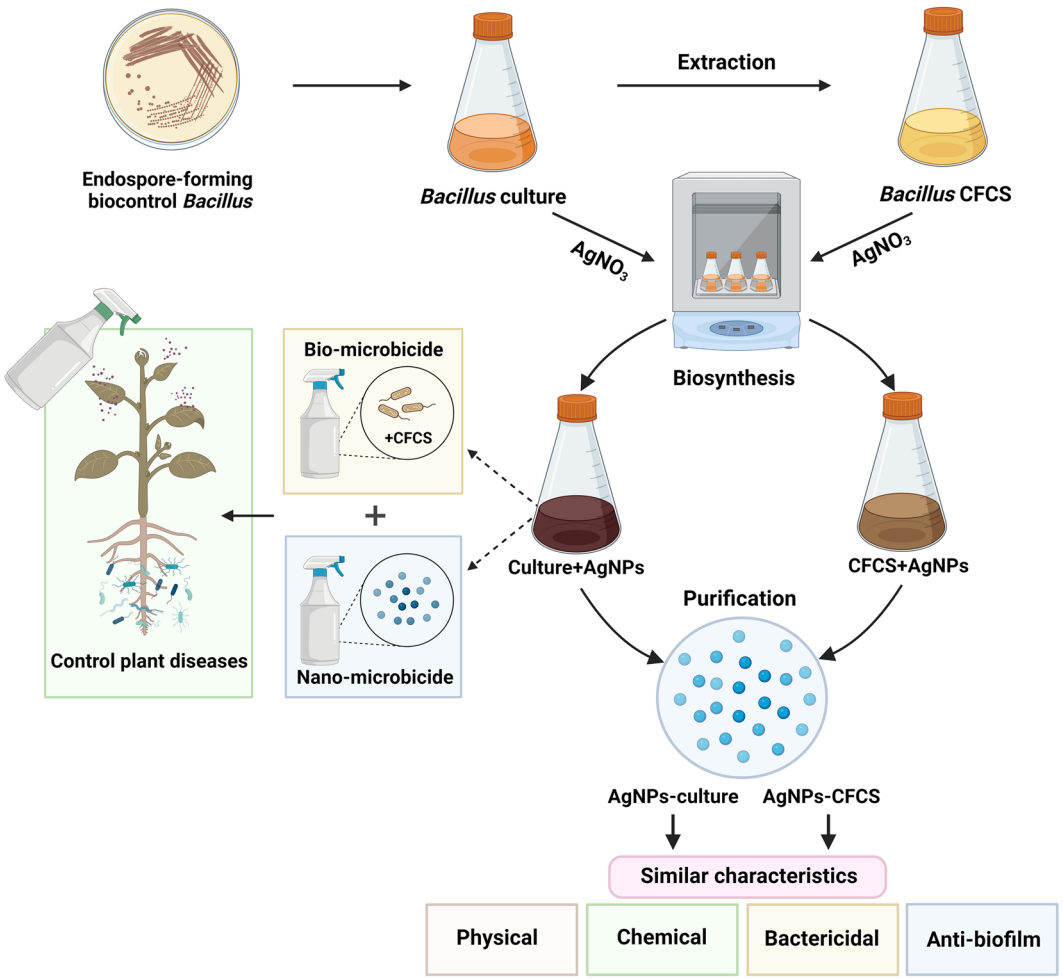

Introduction

Plant diseases cause enormous reduction in crop yield and quality and heavy burden of using pesticides in modern agriculture. Current plant disease management relies heavily on the use of chemical pesticides, which are compromised by resistance development from target pests and pathogens and environmental toxicity. Nanoparticles with at least one dimension in the range of 1–100 nm have high surface-to-volume ratios and display exceptional physical and chemical properties compared with their molecular and bulk counterparts [50]. Metal and metal oxide nanoparticles have shown potent pesticide-activities through multiple mechanisms and are hard for pests and pathogens to develop

resistance, leading to increased pesticide efficacy and durability and reduced dosage and risks and thus becoming one type of promising nanopesticides [3, 28, 47].

Metal and metal oxide nanoparticles have been synthesized by various physical and chemical methods, such as ultrasonication, microwave irradiation, thermal or laser ablation, electrochemistry, chemical reduction, and photochemical reduction, which have the disadvantages of requiring high energy, using expensive equipment or toxic chemicals, and producing less biocompatible products [15, 35, 42]. Biological green synthesis of nanoparticles under ambient temperature and pressure using ecofriendly reducing and stabilizing materials from microbes and plants without using toxic chemicals reduces health and environmental risks at source level, produces nanoparticles with higher stability and biocompatibility, and promotes the sustainable use of nanoparticles [15, 35, 42]. Currently, the major bottleneck in the development and commercialization of biological green synthesis of nanoparticles is the large-scale production of nanoparticles, requiring not only large reactors to produce large-scale nanoparticles but also large facilities to prepare large-scale raw materials of biomass or cell-free extracts of microbes or plants and to purify nanoparticle products, the upstream and downstream processes which are laborious and expensive [15, 35].

Biological control using antagonistic microbes against pathogens and pests is an alternative to the application of chemical pesticides. Gram-positive endospore-forming bacteria belonging to the Subtilis clade within the genus *Bacillus* [18] can produce multifarious secondary metabolites against broad plant pathogens and produce endospores resistant to heating and dryness for the formulation of stable products, and thus are high-profile biocontrol agents [12, 44, 51]. Some of these biocontrol *Bacillus* strains or their culture filtrate or supernatant can mediate the synthesis of metal or metal oxide nanoparticles having microbicidal and insecticidal activities [13, 21, 24, 36]. *Bacillus* usually forms endospores in response to nutritional and environmental stresses [34]. *Bacillus* cells in cultures at the stationary phase under nutrient starvation form endospores and probably become resistant to heavy metal ions (e.g., Ag^+) and metal nanoparticles (e.g., silver nanoparticles, AgNPs). Likely, biocontrol *Bacillus* cells in culture can survive after forming endospores, while the aqueous part of the culture containing *Bacillus*-produced and -released extracellular reducing and stabilizing substances undergoes the synthesis of metal nanoparticles from metal solution or suspension; the survived biocontrol *Bacillus* cells and the *Bacillus* culture-mediated product of metal nanoparticles can work as synergistic bio-microbicide and nano-microbicide to control phytopathogens and plant diseases.

Bacillus amyloliquefaciens strain A3 is such an endospore-forming biocontrol bacterium that has antagonistic activities against broad-spectrum phytopathogenic fungi and bacteria [11, 22] and can produce and release substances mediating reduction of Ag^+ to Ag^0 and stabilization of AgNPs [21]. Its cell-free culture supernatant (CFCS) and CFCS-mediated AgNP product (AgNP–CFCS) have shown synergistic antibacterial activities [21].

In this study, we chose the *B. amyloliquefaciens* strain A3 to produce the synergistic bio-microbicide and nano-microbicide together to control the bacterial pathogen *Pseudomonas syringae* pv. *actinidiae* (Psa) causing the bacterial canker disease of kiwifruit plants. This study provides a solution to save the troubles of extraction, separation, and purification in the green synthesis of antimicrobial nanoparticles using cell-free extracts of bacteria by using endospore-forming *Bacillus* biocontrol agents to produce bio-microbicide and nano-microbicide together and use them together.

Materials and methods

Bacteria and media

Bacillus amyloliquefaciens strain A3 was isolated from rice seeds and has shown antagonistic activities against multiple phytopathogenic fungi and bacteria [11, 22]. Psa strains T6-1 and ML2-12 were isolated from bacterial canker stems of kiwifruit plants grown in Taizhou, China and cause the bacterial canker disease of kiwifruit plants [4].

Bacteria were cultured in a nutrient broth (containing sucrose 10 g, tryptone 10 g, peptone 3 g, and yeast extract 1 g per liter; pH 7.0) and on the solidified nutrient agar medium containing agar 15 g per liter.

Preparation of cell-free culture supernatant (CFCS) of *B. amyloliquefaciens*

A single colony of strain A3 grown on the nutrient agar at 30 ℃ for 24 h was inoculated into the nutrient broth and cultured at 30 ℃ and 180 rpm for 24 h. The cell concentration of the bacterial suspension was measured by optical density (OD) at 600 nm (OD600) and adjusted to OD600 = 1 using sterile distilled water. One milliliter of the bacterial suspension at OD600 = 1 was inoculated into 100 mL of the nutrient broth in a 500-mL Erlenmeyer flask and cultured at 30 ℃ and 180 rpm for 48 h. The culture of strain A3 appeared in orange red was centrifugated at 3050 g for 15 min; the supernatant was centrifugated at 10,000*g* for 10 min; then, the supernatant was used as CFCS. No bacterium in the CFCS was

confirmed by no bacterial growth after incubating 100 µL of the supernatant on the nutrient agar at 30 ℃ for 24 h.

Biosynthesis of AgNPs using CFCS (AgNP–CFCS)

Three milliliters of $AgNO_3$ solution (100 mM) were added into the CFCS obtained from a 48-h culture in a 500-mL Erlenmeyer flask to a final concentration of 3 mM and then shaken at 180 rpm at 30 ℃ for 24 h. The nutrient broth (100 mL) containing 3 mM of $AgNO_3$ in the 500-mL Erlenmeyer flask was used as control. The synthesis of AgNPs was indicated by color change from light yellow to dark brown [20] and then determined by UV–visible spectrometry. The dark brown colloid (1 mL) was diluted 30-time with Milli-Q water and scanned from 200 to 800 nm at 1 nm resolution using a Shimadzu UV-2550 spectrometer (Shimadzu, Kyoto, Japan). Standard AgNP (10–15 nm) colloid (Aladdin Biochemical Technology, Shanghai, China) at concentrations from 10 to 2 $\mu g \cdot mL^{-1}$ was prepared to establish the standard curve for the UV–visible spectrometry to determine the concentration of AgNPs; CFCS was used as blank to set the baseline of the UV–visible spectra. The AgNP–CFCS were purified via centrifugation at 27,200*g* for 10 min, washed twice with Milli-Q water and then freeze-dried.

Biosynthesis of AgNPs using *B. amyloliquefaciens* culture (AgNP-culture)

Three milliliters of $AgNO_3$ solution (100 mM) were added into 100 mL of the 48-h culture of strain A3 in a 500-mL Erlenmeyer flask and then shaken at 180 rpm at 30 ℃ for 24 h. The nutrient broth (100 mL) containing 3 mM of $AgNO_3$ in the 500-mL Erlenmeyer flask was used as control. The synthesis of AgNPs was indicated by color change from orange–red (color of strain A3) to light brown and then determined by UV–visible spectrometry. The AgNP-culture were purified by centrifugation of the bacterial culture at 3050*g* for 15 min and then centrifugation of the supernatant at 27,200*g* for 10 min; the pellet was washed twice with Milli-Q water and then freeze-dried.

Survive of endospore-forming *B. amyloliquefaciens* exposing to $AgNO_3$ and AgNPs

The numbers of alive bacterial cells in the 48-h culture of strain A3 and after the biosynthesis of AgNPs were determined by plating culture after serial dilution. After heating 5 mL of bacterial suspension in water bath at 80 ℃ for 10 min, the numbers of heat-tolerant endospore-forming *B. amyloliquefaciens* cells in the 48-h culture and after the biosynthesis of AgNPs were determined by plating culture after serial dilution. Three plates were prepared for each dilution. This experiment was done twice.

Physical characterization of AgNPs

The size and morphology of AgNPs were observed by transmission electron microscopy. The purified AgNPs were ultrasonically dispersed in Milli-Q water to colloidal AgNPs at 100 $\mu g \cdot mL^{-1}$. One drop of colloidal AgNPs was applied onto a carbon-coated copper grid and dried under a lamp. The AgNPs carried by the grid were observed with a JEM-1400 transmission electron microscope (JEOL, Tokyo, Japan). The diameters of 200 arbitrarily selected AgNPs in micrographs were measured using the Nano Measurer 1.2 software developed by Department of Chemistry, Fudan University (https://nano-measurer.software.informer.com/1.2/).

The crystalline nature of AgNPs was analyzed by X-ray diffraction spectroscopy. The AgNP powder was mounted on a film-coated glass slide and analyzed using a D8 Advance Diffractometer (Bruker, Karlsruhe, Germany) in the 2θ range from 0° to 90° with Cu-Kα radiation at 40 kV and 40 mA.

Chemical and electrical characterization of AgNPs

The Ag element of AgNPs was detected by energy-dispersive X-ray spectroscopy. The AgNP powder was mounted on a double-sided adhesive conductive carbon tape. The Ag element was detected at 20 keV by an X-Max N energy-dispersive spectrometer (Oxford Instruments, Oxford, UK) attached to a Gemini-iSEM 300 scanning electron microscope (Carl Zeiss, Oberkochen, Germany).

The functional groups responsible for the synthesis and stabilization of the AgNPs were detected by Fourier transform infrared (FT-IR) spectroscopy. The AgNP powder (1 mg) was mixed with KBr (100 mg) and compressed to a thin pellet by hydraulic pellet press. The CFCS and the 48-h culture of strain A3 were freeze-dried and ground to powders, which were also mixed with KBr and compressed to a thin pellet. The FT–IR spectra were recorded in the range of 500–4000 cm^{-1} with a resolution of 4 cm^{-1} using a Nicolet iS50FT–IR spectrometer (Thermo Scientific, Madison, USA) and were interpreted using the table of Bruker infrared (Bruker Optics Inc., Billerica, MA, USA) and the absorption table of Libre Texts infrared spectroscopy (https://chem.libretexts.org/).

The zeta potential of the colloidal AgNPs was measured using a Malvern Zeta-sizer Nano ZS90 system (Malvern Instruments, Worcestershire, UK) at 25 ℃.

Bactericide assay for AgNPs against Psa

Psa strains were cultured in the nutrient broth to the mid-exponential phase and were adjusted with the nutrient broth to a suspension about 5×10^8 $CFU \cdot mL^{-1}$.

The antibacterial activity of AgNPs against Psa growth was determined by monitoring bacterial OD600 and detecting bacterial viability using live/dead staining of nucleic acids. In test tubes containing 4.8 mL of the nutrient broth, 0.6 mL of the suspension of Psa strain ML2-12 or T6-1 were added, and then 0.6 mL of sterile Milli-Q water (control), CFCS, 1 mM $AgNO_3$ solution, 0.1 mM colloidal AgNP–CFCS, or 0.1 mM colloidal AgNP-culture were added. The Psa cultures (6.0 mL) were shaken at 200 rpm and 30 °C for 24 h. Afterwards, 200 µL of the cultures were transferred into wells of a 96-well microplate and OD600 was measured using a SpectraMax Plus 384 spectrophotometer (Molecular Devices, Sunnyvale, CA, USA). The nutrient broth was used as blank. This experiment was done with six replications and repeated three times. Meanwhile, 200 µL of the cultures were transferred into the wells of glass Petri dishes for inverted microscopy and stained in dark for 15 min by nucleic acid dyes NucBeacon Green and propidium iodide from the ViaQuantTM Viability/Cytotoxicity Kit for Bacteria Cells (GeneCopoeia, Rockville, USA). Stained bacterial cells were detected by confocal microscopy using an LSM780 laser scanning confocal microscope (Carl Zeiss, Jena, Germany). Live cells stained by NucBeacon Green were excited at 488 nm and detected at 500–560 nm, while dead cells stained by propidium iodide were excited at 514 nm and detected at 580–660 nm. This experiment was done with three replications and repeated once.

Anti-biofilm assay for AgNPs against Psa

The anti-biofilm activity of AgNPs against Psa was determined by crystal violet staining of biofilm and propidium iodide staining of dead cells. In wells of a 96-well microplate (Corning-Costar Crop., Corning, USA) containing 90 µL of the nutrient broth, 10 µL of the suspension of Psa strain ML2-12 or T6-1 were added, and then 100 µL of sterile Milli-Q water (control), 20 µM colloidal AgNP–CFCS, or 20 µM colloidal AgNP-culture were added. The Psa cultures (200 µL) were incubated 30 °C for 24 h. The nutrient broth was used as blank. Afterwards, the liquid in the wells was removed and the wells were washed three times with distilled water.

Bacterial cells attached to the wells were fixed by 95% methanol (200 µL) for 15 min and then stained with 0.1% (w/v) crystal violet (200 µL) for 15 min at room temperature. The wells were then washed thoroughly with distilled water and air-dried for 2 h. The crystal violet dye that stained the bacterial cells in the wells was dissolved with 33% (v/v) acetic acid (200 µL) and transferred to a fresh microplate. The absorbance of the crystal violet solution was measured at 590 nm (OD590). This experiment was done with six replications and repeated three times.

Meanwhile, bacterial cells attached to the wells were stained by propidium iodide in phosphate buffer saline (200 µl) for 20 min and then were detached from the wells by sterile cotton swabs. The bacterial suspensions were analyzed by flow cytometry using a BD FACSVerse™ system (BD Biosciences, San Jose, USA). This experiment was done with three replications and repeated twice.

Assays on bio-microbicide and nano-microbicide against Psa

The potential of controlling the bacterial canker disease of kiwifruit plants by the bio-microbicide (strain A3 and CFCS) and nano-microbicide (AgNP-culture and AgNP–CFCS) were tested with Psa strain T6-1 and detached leaves of kiwifruit plants (*Actinidia chinensis* var. *deliciosa* 'Hayward'). Healthy leaves were collected from 4-week-old seedlings of the cultivar Hongyang. Detached leaves were surface sterilized by immersing in 70% (v/v) ethanol for 1 min and then 0.6% (w/v) sodium hypochlorite for 3 min, and washing six times with sterile water, and then were air-dried inside a clean bench. Psa strain T6-1 was cultured in the nutrient broth to the mid-exponential phase and then cells were washed with sterile water and adjusted to a suspension about 5×10^8 CFU·mL^{-1}. The Psa suspension (0.6 mL) was sprayed over the air-dried leaves and air-dried again inside a clean bench. The air-dried leaves sprayed with sterile water and then air-dried were used as non-inoculated control. CFCS containing the AgNP product and the strain A3 culture containing the AgNP product were diluted 20 times and 200 times (containing about 0.01 mM AgNPs) with sterile water and 1 mL of each dilution was sprayed over the air-dried leaves. The air-dried leaves sprayed with sterile water were used as inoculated control. Each leaf was kept on two layers moistened filter papers inside a 15-cm Petri dish. The leaves were kept under 26 ℃, a 16-h light (210 µmol·m^{-2}·s^{-1}) and 8-h dark photoperiod, and 75% relative humidity in a growth chamber for 7 d. The percentage of Psa lesion area in leaves was calculated using the ImageJ software (https://imagej.net/ij/). This experiment was done with six replications and repeated three times.

Statistical analyses

All data are presented as mean ± SD (standard deviation) using Microsoft Excel 2019. One-way analysis of variance (ANOVA) test was done using the SPSS software version 21 (SPSS, Chicago, USA) and the significance level was set at $p < 0.05$.

Results and discussion

Most *B. amyloliquefaciens* formed endospores and survived after exposing to $AgNO_3$ and AgNPs

The number of alive bacterial cells in the 48-h culture of strain A3 was $1.74 \pm 0.04 \times 10^9$ CFU·mL^{-1} and 84% of the strain A3 cells ($1.46 \pm 0.06 \times 10^9$ CFU·mL^{-1}) formed endospores and tolerated the heating at 80 ℃ for 10 min. Likely, strain A3 cells in the 48-h culture were at the stationary phase under a nutrient starvation and thus most cells formed endospores.

After exposing strain A3 cells to 3 mM $AgNO_3$ and newly synthesized AgNPs for 24 h, about 87% of the strain A3 cells forming endospores survived and were able to tolerate the heating at 80 ℃ for 10 min. Clearly, most strain A3 cells survived after the biosynthesis of AgNPs.

Before using the strain A3 to produce bio-microbicide and nano-microbicide, we did a screening on 21 strains belonging to the Subtilis clade of the genus *Bacillus* [22] and found that all strains at the stationary phase formed endospores and tolerated Ag^+ (3 mM) but, besides the strain A3, only two strains (*B. amyloliquefaciens* strain D29 and *B. subtilis* strain A15) [13] produced AgNPs from $AgNO_3$ in the nutrient broth cultures. Therefore, the coproduction of bio-microbicide and silver nano-microbicide mediated by the endospore-forming *Bacillus* requires a screening on the biocontrol *Bacillus* agents for the culture-mediated production of AgNPs (AgNP-culture).

AgNP-culture and AgNP–CFCS display similar physical and chemical characteristics

UV–visible spectroscopy revealed the characteristic surface–plasmon–resonance peak of AgNPs at 411 nm and 413 nm produced in CFCS and culture of strain A3, respectively, despite their different colors (dark brown and light brown) in the liquid media (Fig. 1a, b).

A standard curve ($y = 0.1667x - 0.01945$; $R^2 = 0.9981$) was established for the quantification of AgNP concentrations using UV–visible spectroscopy, where x is the concentration of AgNP, y is the absorbance unit at the surface–plasmon–resonance peak. The concentration of AgNPs produced in CFCS was 199 μg·mL^{-1} (1.84 mM) and the yield was 61.4%.

Transmission electron microscopy showed that purified AgNP–CFCS and AgNP-culture were in spherical or nearly spherical morphology and the morphology appeared to be more defined in the AgNP-culture than the AgNP–CFCS (Fig. 1c, d). The average diameter of the AgNP–CFCS (6 – 30 nm) and AgNP-culture (6–28 nm) was 13.29 ± 0.26 nm and 11.10 ± 0.28 nm, respectively (Fig. 1e, f).

X-ray diffraction spectra showed that the purified AgNP–CFCS and AgNP-culture had five characteristic Bragg-reflection peaks (1 0 1), (1 1 1), (2 0 0), (2 2 0), and (3 1 1) at 2θ values 32.20° and 32.21°, 37.99° and 38.07°, 46.20° and 46.13°, 67.49° and 67.46°, and 77.14° and 76.71°, respectively (Fig. 1g, h). The X-ray diffraction spectra indicate crystalline planes of the face-centered cubic silver based on the standard powder diffraction card of Ag^0 (JCPDS Card no. 04–0783) in the Joint Committee on Powder Diffraction Standards library. The unassigned peaks at 2θ values 27.79° and 27.80°, 54.89° and 54.78°, 57.25° and 57.30° (asterisks in Fig. 1g, h) may correspond to the biomolecules coating the AgNPs.

The average particle sizes of the AgNP–CFCS (13.34 nm) and AgNP-culture (11.58 nm) can be calculated using the Debye–Scherrer formula: $D = K\lambda/(\beta \text{Cos}\theta)$, where D is the diameter of coherent diffraction domain, K is the Scherrer constant (0.94), λ is the X-ray wavelength (0.15406 nm), β is the full-width at half maximum of the X-ray diffraction peak, and θ is the diffraction angle corresponding to the lattice plane (1 1 1) [31]. The calculated average diameters of the AgNP–CFCS and AgNP-culture are close to the corresponding values measured from the electron micrographs (Fig. 1e, f).

Energy-dispersive spectroscopy revealed typical optical absorption peak of Ag element at about 3 keV [20, 21] (Fig. 2a, b). The weight percentage of Ag in AgNP–CFCS and AgNP-culture is 55.0% and 64.6%, respectively. The second predominant element is C in AgNP–CFCS (22.4 wt%) and AgNP-culture (13.2 wt%). The AgNPs also contain Cl, O, and N from media and strain A3.

The presence of functional groups responsible for the reduction of Ag^+ and the stabilization of AgNPs in

(See figure on next page.)

Fig. 1 Physical characterization of silver nanoparticles (AgNPs) synthesized with *Bacillus amyloliquefaciens* strain A3. Cell-free culture supernatant (CFCS) was obtained from the culture of strain A3 grown in a nutrient broth for 48 h. AgNP–CFCS is AgNPs produced in the CFCS with 3 mM $AgNO_3$ for 24 h. AgNP-culture is AgNPs produced in the 48-h culture with 3 mM $AgNO_3$ for 24 h. **a**, **b** UV–visible spectra of AgNPs. **c**, **d** Transmission electron micrographs show spherical and nearly spherical AgNPs. **e**, **f** Histograms of the diameter distribution of the AgNP–CFCS and AgNP-culture in the micrographs. **g**, **h** X-ray diffraction spectra show the nanoscale size and crystalline nature of AgNPs. The five diffraction peaks (101), (111), (200), (220) and (311) at the respective 2θ degree 32.20° and 32.21°, 37.99° and 38.07°, 46.20° and 46.13°, 67.49° and 67.46°, and 77.14° and 76.71° correspond to the lattice plane values of the face-centered cubic silver. The unassigned peaks (asterisks) at 2θ degree 27.79° and 27.80°, 54.89° and 54.78°, 57.25° and 57.30° may correspond to the biomolecules coating the AgNPs

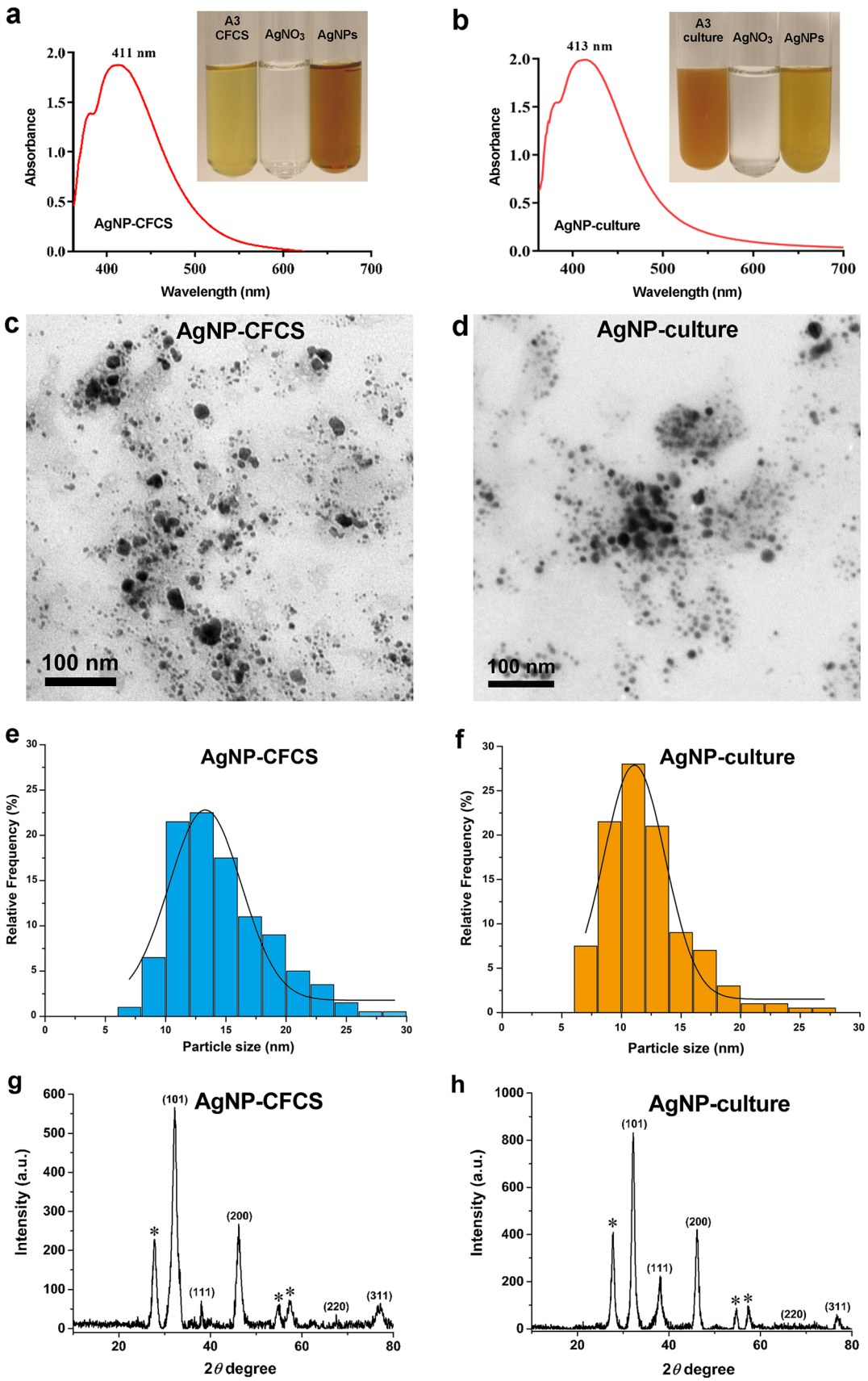

Fig. 1 (See legend on previous page.)

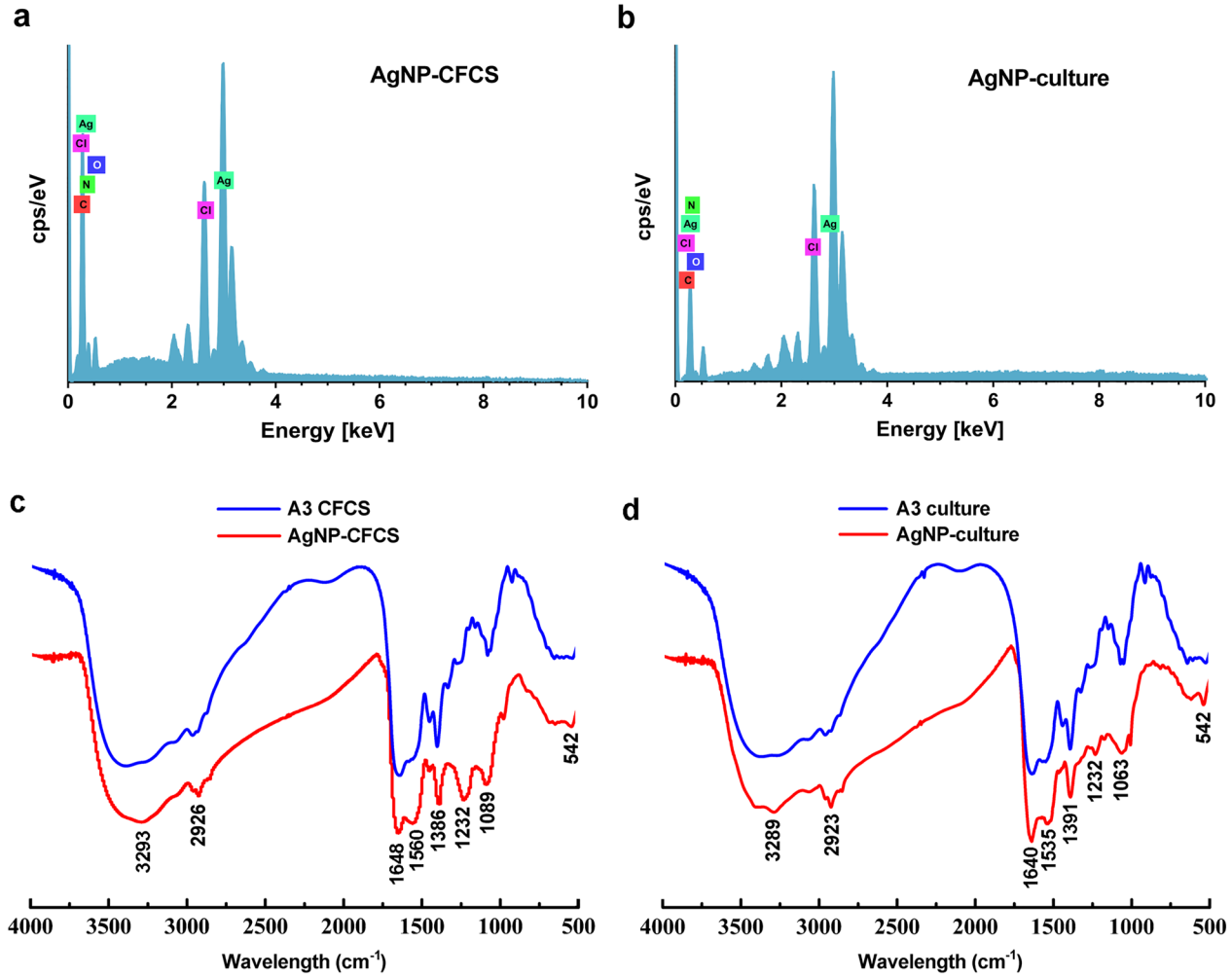

Fig. 2 Chemical characterization of silver nanoparticles (AgNPs) produced in the cell-free culture supernatant (CFCS) (AgNP–CFCS) and in the culture of *Bacillus amyloliquefaciens* strain A3 (AgNP-culture). **a**, **b** Energy-dispersive spectra show major chemical elements in AgNPs. cps/eV: count per second per electron-volt. **c**, **d** Fourier transform infrared spectra show functional groups responsible for the synthesis and stabilization of AgNPs

CFCS and the culture of strain A3 were identified by FT–IR spectroscopy. The FT–IR spectra of CFCS and the culture of strain A3 are similar. The FT–IR spectra of AgNP–CFCS and AgNP-culture are similar and largely like those of CFCS and the culture of A3 (Fig. 2c, d). The FT–IR spectrum of AgNP–CFCS shows absorption at wave numbers 3293, 2926, 1648, 1560, 1386, 1232, 1089, and 542 cm^{-1} (Fig. 2c). The FT–IR spectrum of AgNP-culture shows absorption at wave numbers 3289, 2923, 1640, 1535, 1391, 1232, 1063, and 542 cm^{-1} (Fig. 2d). The peak at 1232 cm^{-1} in AgNPs is distinct from those peaks and bands in CFCS and the culture of strain A3 and is attributed to C–N stretching amine vibration. The bands around 3293 cm^{-1} and 3289 cm^{-1} are attributed to N–H stretching vibrations; the peaks at 2926 cm^{-1} and 2923 cm^{-1} are attributed to C–H stretching vibrations; the peaks at 1648 cm^{-1} and 1640 cm^{-1} are attributed to -C=O carbonyl groups and –C=C stretching vibrations; the peaks at 1560 cm^{-1} and 1535 cm^{-1} are attributed to metal carbonyls stabilizing AgNPs; the peaks at 1386 cm^{-1} and 1391 cm^{-1} are attributed to NO_3^- asymmetrical deformation vibrations [7]; the bands around 1089 cm^{-1} and 1063 cm^{-1} are attributed to C=O stretching vibrations; the band around 542 cm^{-1} is attributed to C–C skeleton vibration. These groups show the presence of peptides and polysaccharides in CFCS and the culture of strain A3 and suggest that these functional groups reduce Ag^+ to synthesize AgNPs and bind to AgNPs to stabilize the nanoparticles.

Zeta potential, the electrical potential between the inner Helmholtz layer near a particle surface and the particle-suspended bulk liquid, indicates the potential stability of a colloidal system. Colloids with high zeta potential (positive or negative) are electrically stabilized,

preventing the particles from aggregation. The value of 25 mV (positive or negative) can be used to separate low-charged surfaces from highly charged surfaces [52]. The zeta potential of AgNP–CFCS and AgNP-culture were − 36.4 ± 4.6 mV and − 35.3 ± 5.2 mV, respectively, indicating moderate stability [52].

AgNP–CFCS and AgNP-culture have shown similar particle size and morphology, crystalline structures, surface–plasmon–resonance peaks, zeta potential, chemical element compositions and organic groups. Therefore, CFCS plays a key role in the synthesis of AgNPs, while strain A3 cells formed endospores in the cultures hardly contribute to the synthesis of AgNPs. X-ray diffraction and FT–IR spectroscopy revealed the biomolecules coating the AgNP–CFCS and AgNP-culture, which is a common feature of AgNPs produced with the extracts of microbes [26, 45, 48] and plants [6, 31, 41, 46].

We modified the recipe of the previous nutrient broth (glucose 2.5 g, tryptone 10 g, beef extract 3 g, and NaCl 5 g per liter) [21] for production of CFCS mediating the synthesis of AgNPs. NaCl was removed to avoid precipitating Ag^+. Sucrose 10 g instead of glucose 2.5 g per liter was used to increase the production of exopolysaccharides [32] which may mediate the reduction and stabilization of AgNPs [27, 29]. FT–IR spectroscopy showed the functional groups associated with AgNPs from polysaccharides and peptides in the CFCS. The modifications of the nutrient broth, the proportioning of CFCS and $AgNO_3$, and culture conditions resulted in smaller sizes of the AgNPs in average diameter about 13 nm comparing with previous 50 nm [21]. The smaller spherical AgNPs with higher surface-to-volume ratios may easily pass through cell membranes [14, 53] and have more potent antibacterial activities.

AgNP-culture and AgNP–CFCS show similar bactericidal activity against Psa

CFCS and $AgNO_3$, the substrates of the AgNP biosynthesis, and the products AgNP–CFCS and AgNP-culture at the respective final concentration 10% (v/v), 0.1 mM, 0.01 mM, and 0.01 mM dramatically inhibited the growth of Psa strains ML2-12 and T6-1 in the nutrient broth. $AgNO_3$ (0.1 mM) and AgNP–CFCS (0.01 mM) showed slightly but significantly greater inhibition on the Psa growth than that by 10% CFCS. AgNP-culture showed the most significant inhibition on the Psa growth (Fig. 3a). After the live/dead staining, confocal microscopy showed that most control Psa cells emitting green fluorescence were live whereas most Psa cells under other treatments were stained by propidium iodide and dead (Fig. 3b). Clearly, 10% CFCS, 0.1 mM $AgNO_3$, 0.01 mM AgNP–CFCS, and 0.01 mM AgNP-culture have bactericidal activity.

AgNP-culture and AgNP–CFCS show similar anti-biofilm activity against Psa

Crystal violet staining and colorimetric assay showed that Psa under AgNP-culture (0.01 mM) and AgNP–CFCS (0.01 mM) formed only 17–24% biofilm on the surface of the polystyrene microplate wells comparing with control (Fig. 4a, b). Moreover, propidium iodide staining and flow cytometry revealed that AgNP-culture and AgNP–CFCS killed 40–50% Psa cells embedded in the biofilms (Fig. 4c, d).

Bio-microbicide and nano-microbicide together protect kiwifruit leaves from Psa infection

Seven days after inoculation, Psa T6-1 caused lesions occupied 22% of leaf area. The 200-time diluted bio-microbicide and nano-microbicide products (CFCS containing AgNPs and strain A3 culture containing AgNPs) dramatically reduced the lesion area to 5% of the leaf area, while the 20-time diluted products almost eliminated Psa lesions (Fig. 5). The bio-microbicide (strain A3 and CFCS) and nano-microbicide (AgNP-culture and AgNP–CFCS) together protected kiwifruit leaves from Psa infection.

AgNP–CFCS and AgNP-culture have shown similar bactericidal and anti-biofilm activities. Moreover, the 200-time or 20-time diluted CFCS and strain A3 culture containing AgNPs have shown almost identical control efficiency against Psa infection in kiwifruit leaves. Likely, AgNPs, Ag^+, and antibacterial substances in the CFCS but not the dormant strain A3 cells played the major role in rapid control of the Psa infection, while CFCS played the role of bio-microbicide. The strain A3 cells on leaves may act as a biocontrol agent after recovery.

Bacteria in natural environments usually attach to surfaces and exist as multicellular assemblies in a structured, protective biofilm matrix [39]. Plant pathogenic bacteria, such as Psa, colonize in biofilms outside and inside plant tissues [16, 40], protecting them from host defenses and bactericides [8]. Psa has developed resistance to the conventional bactericidal streptomycins and copper compounds and thus urges the development of more effective antibacterial agents against Psa biofilm [8]. Here, we show the potent anti-biofilm activities of AgNPs against Psa via inhibition of biofilm formation and damage of Psa cells embedded in the biofilm matrix. Moreover, strain A3 produces lipopeptide surfactins, which have exceptional surfactant activity [33, 38], and showed potent bactericidal activity and anti-biofilm activity against the phytopathogen *Dickeya dadantii* [22]. Therefore, the application of the synergistic bio-microbicide (strain A3 culture) and nano-microbicide (AgNPs) appears to be an effective solution in the management of the bacterial canker disease of kiwifruit plants in future.

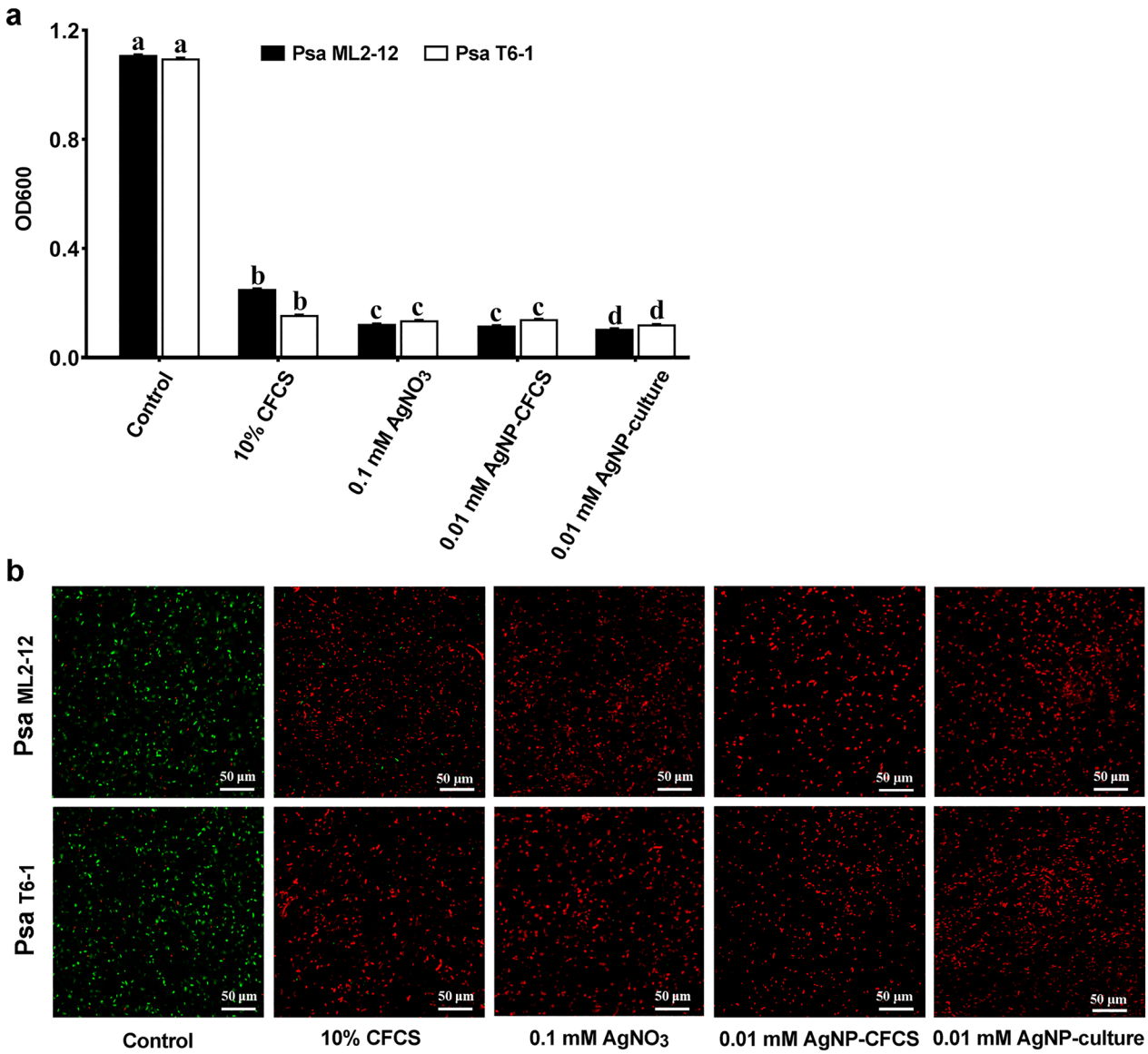

Fig. 3 Bactericidal activities of CFCS, $AgNO_3$, AgNP–CFCS, and AgNP-culture against *Pseudomonas syringae* pv. *actinidiae* (Psa) strains ML2-12 and T6-1. **a** Psa grown in nutrient broth containing 10% (v/v) CFCS, 0.1 mM $AgNO_3$, 0.01 mM AgNP–CFCS, and 0.01 mM AgNP-culture indicated by optical density at 600 nm (OD600). Data are presented as mean values with standard deviation (vertical bars); the different letters on the vertical bars indicate significant difference between treatments according to one-way analysis of variance at the significance level $p < 0.05$. **b** Images of confocal microscopy show Psa cells grown in nutrient broth containing CFCS, $AgNO_3$, AgNP–CFCS, and AgNP-culture after staining by nucleic acid dyes NucBeacon Green and propidium iodide. Live cells stained by NucBeacon Green are presented in green, while dead cells stained by propidium iodide are presented in red

At present, two risk factors, small-size AgNPs (< 20 nm in diameter) and non-transformed Ag^+, hinder the application of this synergistic bio-microbicide and nano-microbicide in fields. In general, AgNPs < 20 nm in diameter are toxic to living organisms [17, 25, 30, 53]. Rush application of this synergistic bio-microbicide and nano-microbicide containing toxic AgNPs and Ag^+ may cause adverse effects on living organisms and environment. Increasing the size of the AgNP product > 20 nm in diameter and the transformation rate of Ag^+ to Ag^0 is a solution to reduce the toxic risk of using the synergistic bio-microbicide and nano-microbicide. On the other hand, the green process and green product developed in this study reduce the toxic risk. First, negatively charged nanoparticles are less cytotoxic and genotoxic to mammalian cells than positively charged nanoparticles [10,

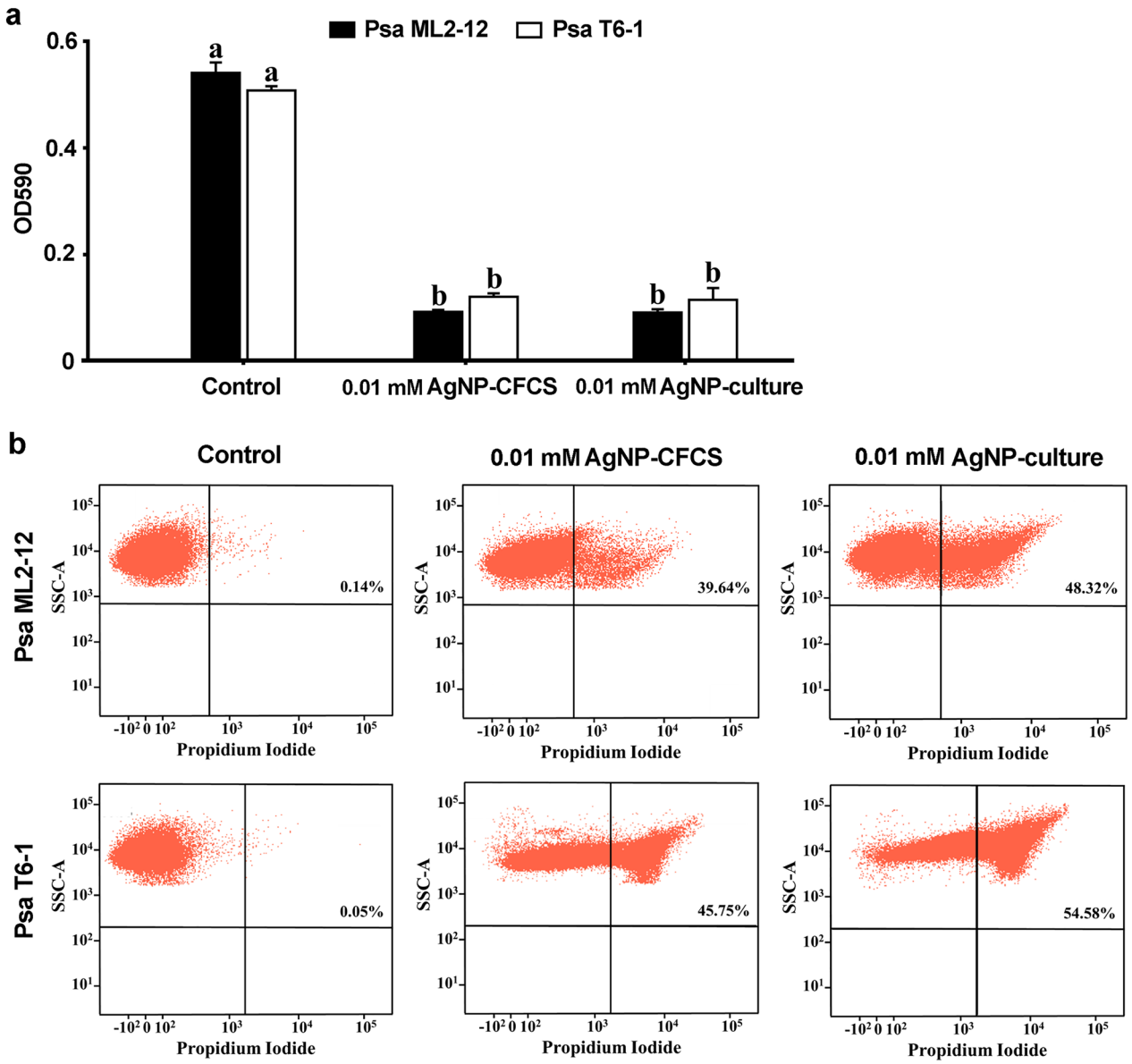

Fig. 4 Anti-biofilm activities of AgNP–CFCS and AgNP-culture against Psa strain ML2-12 and T6-1 determined by crystal violet staining of biofilms and propidium iodide staining of dead cells. **a** Absorbance of crystal violet at 590 nm (OD590) indicates Psa cells in biofilms. Data are presented as mean values with standard deviation (vertical bars); the different letters on the vertical bars indicate significant difference between treatments according to one-way analysis of variance at the significance level $p < 0.05$. **b** Flow cytometry analyses show dot plots of fluorescence signals from dead Psa cells stained by propidium iodide against sideward scatter (SSC), indicate percentage of dead cells in total cells of the biofilms formed under AgNPs

23] which may be internalized by mammalian cells at a high rate [1]. Second, the green synthesis generates biomolecules coating the AgNPs, reducing the toxicity of AgNPs to living organisms and environment by preventing exposure of Ag^0 to oxidation and slow release of toxic Ag^+ [9]. Third, the synergistic action of the bio-microbicide and nano-microbicide can reduce the working concentration of AgNPs and Ag^+.

Conclusions

To realize the full potential of nanotechnology-enabled sustainable agriculture, such as using nanopesticides of metallic nanoparticles in plant protection, three major barriers need to be overcome: scale up production and delivery at field scale, regulatory and safety concerns, and consumer acceptance [19]. Here, we tried to scale

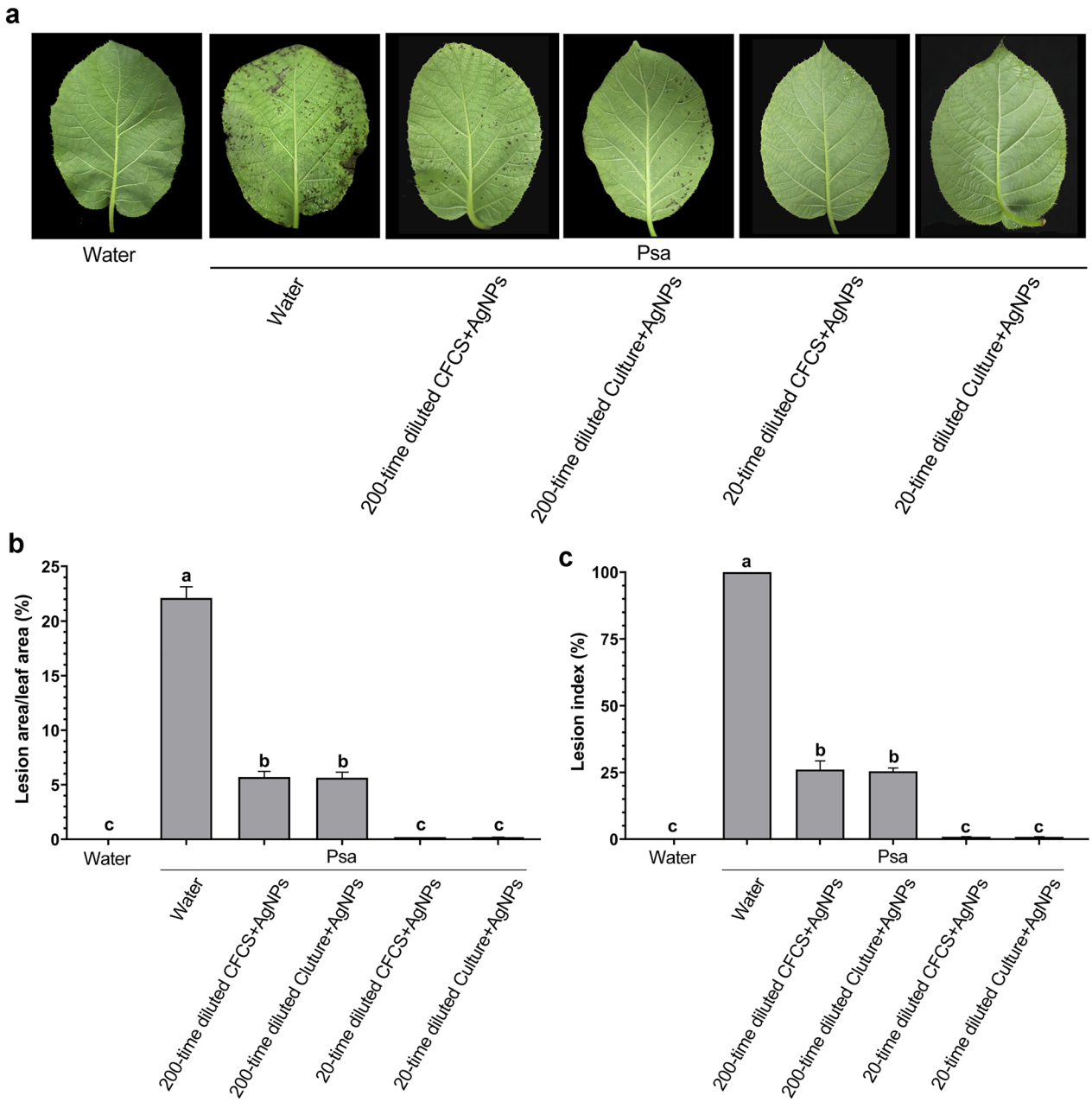

Fig. 5 CFCS and AgNPs protect kiwifruit leaves from infection by Psa strain T6-1. **a** Representative kiwifruit leaves under different treatments. Bacterial suspension (0.6 mL of 5×10^8 CFU·mL^{-1}) containing 3×10^8 Psa cells was sprayed over each leaf. Leaves sprayed with sterile water were used as non-inoculated control. CFCS containing the AgNP product (CFCS + AgNPs) and culture of *Bacillus amyloliquefaciens* strain A3 containing the AgNP product (Culture + AgNPs) were diluted 20 and 200 times (containing about 0.01 mM AgNPs) with sterile water and 1 mL of each dilution was sprayed over the inoculated leaves. Inoculated leaves sprayed with sterile water were used as inoculated control. **b** 7 days after inoculation, percentage of lesion area in leaves was calculated using ImageJ. **c** Lesion index (%) is the percentage of lesion area comparing with that in the inoculated control leaves, which is set to 100%. Data are presented as mean values with standard deviation (vertical bars); the different letters on the vertical bars indicate significant difference between treatments according to one-way analysis of variance at the significance level $p < 0.05$

up the green production of metal nanoparticles to overcome the first barrier.

The process of biological green synthesis of nanoparticles generally includes preparation of biomass or cell-free extracts of microbes or plants, one-pot synthesis of nanoparticles, and purification of the nanoparticle products. The one-pot synthesis is comparatively energy- and cost-effective whereas the preparation of biological raw

materials and the purification of nanoparticle products are generally laborious, expensive, and difficult to scale up. Here, we simplified the process of biological green synthesis to a one-pot synthesis alone by changing the way of using nanoparticles alone to use the nano-microbicide products together with the biological raw materials as bio-microbicides to control phytopathogens and plant diseases, and thus save the troubles of extraction, separation, and purification. The key to the strategy is using endospore-forming biocontrol bacteria which can tolerate nano-microbicide and produce substances mediating the synthesis of the nano-microbicide, requiring a screening on the endospore-forming biocontrol agents for the culture-mediated production of nano-microbicide. The high-profile biocontrol bacteria belonging to the *Bacillus subtilis* clade [18, 51] and the *Paenibacillus polymyxa* complex [5, 37] are promising candidates for the screening.

This study demonstrates that the *B. amyloliquefaciens* strain A3 can tolerate Ag^+ and AgNPs after forming endospores and its culture has produced and released substances into the CFCS to mediate the synthesis of AgNPs. Consequently, AgNPs produced from the *Bacillus* culture and CFCS show similar physical, chemical, and electrical characteristics, and bactericidal and antibiofilm activities.

The one-pot coproduction of the bio-microbicide and nano-microbicide developed at the laboratory scale can be easily scaled up based on the existing liquid fermentation processing of the *Bacillus* biocontrol agent. For example, when the *Bacillus* cells have formed endospores at the final stage of the liquid fermentation, a small volume of a high-concentration $AgNO_3$ solution will be added in the stirred tank bioreactor to produce AgNPs by continuous stirring for certain time. This coproduction of bio-microbicide and nano-microbicide is a totally green one-pot synthesis process without production of waste. The liquid product containing bio-microbicide and nano-microbicide can be used after dilution to control plant diseases.

We used AgNP as the nano-microbicide because AgNPs are the most widely and commercially used metal nanoparticles in daily products, highly effective nano-microbicide, and easy for monitoring of biosynthesis via color change. This pilot study verified the feasibility of using the endospore-forming *Bacillus* bacteria tolerating Ag^+ and AgNPs to produce bio-microbicide and nano-microbicide in one pot. The coproduction and cooperation of bio-microbicide and nano-microbicide can be easily scaled up by using the existing liquid fermentation processing and foliar spray at field scale for a *Bacillus* biocontrol agent. However, the high cytotoxic and genotoxic potential of Ag^+ and AgNPs require high regulatory and safety concerns. Determining the real risk of the AgNPs releasing into the environment is technically difficult and has not been fully assessed so far. Previous studies have not got a concrete idea on the toxicity of AgNPs to living organisms and environment [2, 43]. Future studies should determine the efficiency of AgNPs in plant protection in fields along with the assessment of their potential risks to environment, food safety, and human health by experimental assessment and mathematical modelling [49]. Alternatively, the strategy of the coproduction and cooperation of bio-microbicide and nano-microbicide can be realized by using biologically benign and generally recognized as safe (GRAS) materials, such as endospore-forming biocontrol agents belonging to the *Bacillus subtilis* clade and the *Paenibacillus polymyxa* complex and Zn-based nanomaterials [37], which are typically subjected to lower regulatory scrutiny.

Acknowledgements
The authors extend their appreciation for the Deputyship for Research and Innovation, Ministry of Education in Saudi Arabia (IFKSUOR3-235-1).

Author contributions
YY: investigation, methodology, formal analysis, visualization, and writing—original draft. CW: investigation, methodology, formal analysis, and writing—original draft. YA: methodology, formal analysis, and data curation. QL: investigation and methodology. CL: investigation. JL: conceptualization, funding acquisition, and project administration. DD: conceptualization, funding acquisition, and project administration. SSA-R: funding acquisition, visualization, and resources. MM: funding acquisition, visualization, and resources. BL: conceptualization, funding acquisition, and supervision. SOO: funding acquisition, visualization, and supervision. QA: conceptualization, validation, visualization, supervision, and writing—original draft. All authors reviewed the manuscript.

Funding
This work was supported by the Key Research and Development Program of Zhejiang Province, China (2020C02006), the Shanghai Agriculture Applied Technology Development Program (2021-02-08-00-12-F00771), and the Deputyship for Research and Innovation, Ministry of Education in Saudi Arabia (IFKSUOR3-235-1).

Declarations

Ethics approval and consent to participate
Not applicable.

Consent for publication
Not applicable.

Competing interests
The authors declare that they have no competing interests.

Author details
[1]State Key Laboratory of Rice Biology and Breeding, Key Laboratory of Molecular Biology of Crop Pathogens and Insects Ministry of Agriculture and Rural Affairs, Key Laboratory of Biology of Crop Pathogens and Insects of Zhejiang Province, Institute of Biotechnology, Zhejiang University, Hangzhou 310058, China. [2]Plant Pathology Department, Faculty of Agriculture, Minia University, Elminya 61519, Egypt. [3]Department of Plant Quarantine, Shanghai Extension and Service Center of Agriculture Technology, Shanghai 201103, China. [4]Station for the Plant Protection & Quarantine and Control of Agrochemicals Zhejiang Province, Hangzhou 310004, China. [5]Department of Pharmacology

and Toxicology, College of Pharmacy, King Saud University, P.O. Box 55760, 11451 Riyadh, Saudi Arabia.

Received: 20 September 2023 Accepted: 4 January 2024
Published online: 17 January 2024

References

1. Abdelmonem AM, Pelaz B, Kantner K, Bigall NC, Del Pino P, Parak WJ. Charge and agglomeration dependent in vitro uptake and cytotoxicity of zinc oxide nanoparticles. J Inorg Biochem. 2015;153:334–8. https://doi.org/10.1016/j.jinorgbio.2015.08.029.
2. Akter M, Sikder MT, Rahman MM, Ullah AKMA, Hossain KFB, Banik S, Hosokawa T, Saito T, Kurasaki M. A systematic review on silver nanoparticles-induced cytotoxicity: Physicochemical properties and perspectives. J Adv Res. 2017;9:1–16. https://doi.org/10.1016/j.jare.2017.10.008.
3. Ali MA, Ahmed T, Wu W, Hossain A, Hafeez R, Islam Masum MM, Wang Y, An Q, Sun G, Li B. Advancements in plant and microbe-based synthesis of metallic nanoparticles and their antimicrobial activity against plant pathogens. Nanomaterials. 2020;10:1146. https://doi.org/10.3390/nano10061146.
4. Ali MA, Lou Y, Hafeez R, Li X, Hossain A, Xie T, Lin L, Li B, Yin Y, Yan J, An Q. Functional analysis and genome mining reveal high potential of biocontrol and plant growth promotion in nodule-inhabiting bacteria within *Paenibacillus polymyxa* complex. Front Microbiol. 2021;11: 618601. https://doi.org/10.3389/fmicb.2020.618601.
5. Ali MA, Luo J, Ahmed T, Zhang J, Xie T, Dai D, Jiang J, Zhu J, Hassan S, Alorabi JA, Li B, An Q. Pseudomonas bijieensis strain XL17 within the *P. corrugata* subgroup producing 2,4-diacetylphloroglucinol and lipopeptides controls bacterial canker and gray mold pathogens of kiwifruit. Microorganisms. 2022;10:425. https://doi.org/10.3390/microorganisms10020425.
6. Anbu P, Gopinath SC, Yun HS, Lee CG. Temperature-dependent green biosynthesis and characterization of silver nanoparticles using balloon flower plants and their antibacterial potential. J Mol Struct. 2019;1177:302–9. https://doi.org/10.1016/j.molstruc.2018.09.075.
7. Banu HT, Meenakshi S. Synthesis of a novel quaternized form of melamine–formaldehyde resin for the removal of nitrate from water. J Water Process Eng. 2017;16:81–9. https://doi.org/10.1016/j.jwpe.2016.12.003.
8. Cameron A, Sarojini V. *Pseudomonas syringae* pv. *actinidiae*: chemical control, resistance mechanisms and possible alternatives. Plant Pathol. 2014;63:1–11. https://doi.org/10.1111/ppa.12066.
9. de Souza TAJ, Rosa Souza LR, Franchi LP. Silver nanoparticles: an integrated view of green synthesis methods, transformation in the environment, and toxicity. Ecotoxicol Environ Saf. 2019;171:691–700. https://doi.org/10.1016/j.ecoenv.2018.12.095.
10. El Badawy AM, Silva RG, Morris B, Scheckel KG, Suidan MT, Tolaymat TM. Surface charge-dependent toxicity of silver nanoparticles. Environ Sci Technol. 2011;45:283–7. https://doi.org/10.1021/es1034188.
11. El-shakh AS, Kakar KU, Wang X, Almoneafy AA, Ojaghian MR, Li B, Anjum SI, Xie G-L. Controlling bacterial leaf blight of rice and enhancing the plant growth with endophytic and rhizobacterial *Bacillus* strains. Toxicol Environ Chem. 2015;97:766–85. https://doi.org/10.1080/02772248.2015.1066176.
12. Fira D, Dimkić I, Berić T, Lozo J, Stanković S. Biological control of plant pathogens by *Bacillus* species. J Biotechnol. 2018;285:44–55. https://doi.org/10.1016/j.jbiotec.2018.07.044.
13. Fouad H, Hongjie L, Yanmei D, Baoting Y, El-Shakh A, Abbas G, Jianchu M. Synthesis and characterization of silver nanoparticles using *Bacillus amyloliquefaciens* and *Bacillus subtilis* to control filarial vector *Culex pipiens pallens* and its antimicrobial activity. Artif Cells Nanomed Biotechnol. 2017;45:1369–78. https://doi.org/10.1080/21691401.2016.1241793.
14. Franci G, Falanga A, Galdiero S, Palomba L, Rai M, Morelli G, Galdiero M. Silver nanoparticles as potential antibacterial agents. Molecules. 2015;20:8856–74. https://doi.org/10.3390/molecules20058856.
15. Gahlawat G, Choudhury AR. A review on the biosynthesis of metal and metal salt nanoparticles by microbes. RSC Adv. 2019;9:12944–67. https://doi.org/10.1039/c8ra10483b.
16. Ghods S, Sims IM, Moradali MF, Rehm BH. Bactericidal compounds controlling growth of the plant pathogen *Pseudomonas syringae* pv. actinidiae, which forms biofilms composed of a novel exopolysaccharide. Appl Environ Microbiol. 2015;81:4026–36. https://doi.org/10.1128/AEM.00194-15.
17. Gliga AR, Skoglund S, Wallinder IO, Fadeel B, Karlsson HL. Size-dependent cytotoxicity of silver nanoparticles in human lung cells: the role of cellular uptake, agglomeration and Ag release. Part Fibre Toxicol. 2014;11:11. https://doi.org/10.1186/1743-8977-11-11.
18. Gupta RS, Patel S, Saini N, Chen S. Robust demarcation of 17 distinct *Bacillus* species clades, proposed as novel *Bacillaceae* genera, by phylogenomics and comparative genomic analyses: description of *Robertmurraya kyonggiensis* sp. nov. and proposal for an emended genus *Bacillus* limiting it only to the members of the Subtilis and Cereus clades of species. Int J Syst Evol Microbiol. 2020;70:5753–98. https://doi.org/10.1099/ijsem.0.004475.
19. Hofmann T, Lowry GV, Ghoshal S, Tufenkji N, Brambilla D, Dutcher JR, Gilbertson LM, Giraldo JP, Kinsella JM, Landry MP, Lovell W, Naccache R, Paret M, Pedersen JA, Unrine JM, White JC, Wilkinson KJ. Technology readiness and overcoming barriers to sustainably implement nanotechnology-enabled plant agriculture. Nature Food. 2020;1:416–25. https://doi.org/10.1038/s43016-020-0110-1.
20. Hossain A, Hong X, Ibrahim E, Li B, Sun G, Meng Y, Wang Y, An Q. Green synthesis of silver nanoparticles with culture supernatant of a bacterium *Pseudomonas rhodesiae* and their antibacterial activity against soft rot pathogen *Dickeya dadantii*. Molecules. 2019;24:2303. https://doi.org/10.3390/molecules24122303.
21. Hossain A, Luo J, Ali MA, Chai R, Shahid M, Ahmed T, Hassan MM, Kadi RH, An Q, Li B, Wang Y. Synergistic action of biosynthesized silver nanoparticles and culture supernatant of *Bacillus amyloliquefacience* against the soft rot pathogen *Dickeya dadantii*. Plants. 1817;2023:12. https://doi.org/10.3390/plants12091817.
22. Hossain A, Masum MMI, Wu X, Abdallah Y, Ogunyemi SO, Wang Y, Sun G, Li B, An Q. Screening of *Bacillus* strains in biocontrol of pathogen *Dickeya dadantii* causing stem and root rot disease of sweet potato. Biocontrol Sci Technol. 2020;30:1180–98. https://doi.org/10.1080/09583157.2020.1798356.
23. Huk A, Izak-Nau E, El Yamani N, Uggerud H, Vadset M, Zasonska B, Duschl A, Dusinska M. Impact of nanosilver on various DNA lesions and HPRT gene mutations - effects of charge and surface coating. Part Fibre Toxicol. 2015;12:25. https://doi.org/10.1186/s12989-015-0100-x.
24. Ibrahim E, Fouad H, Zhang M, Zhang Y, Qiu W, Yan C, Li B, Mo J, Chen J. Biosynthesis of silver nanoparticles using endophytic bacteria and their role in inhibition of rice pathogenic bacteria and plant growth promotion. RSC Adv. 2019;9:29293–9. https://doi.org/10.1039/c9ra04246f.
25. Ivask A, Kurvet I, Kasemets K, Blinova I, Aruoja V, Suppi S, Vija H, Käkinen A, Titma T, Heinlaan M, Visnapuu M, Koller D, Kisand V, Kahru A. Size-dependent toxicity of silver nanoparticles to bacteria, yeast, algae, crustaceans and mammalian cells *in vitro*. PLoS ONE. 2014;9: e102108. https://doi.org/10.1371/journal.pone.0102108.
26. John MS, Nagoth JA, Ramasamy KP, Mancini A, Giuli G, Natalello A, Ballarini P, Miceli C, Pucciarelli S. Synthesis of bioactive silver nanoparticles by a *Pseudomonas* strain associated with the Antarctic psychrophilic protozoon *Euplotes focardii*. Mar Drugs. 2020;18:38. https://doi.org/10.3390/md18010038.
27. Kang F, Alvarez PJ, Zhu D. Microbial extracellular polymeric substances reduce Ag^+ to silver nanoparticles and antagonize bactericidal activity. Environ Sci Technol. 2014;48:316–22. https://doi.org/10.1021/es403796x.
28. Kapinder DK, Verma AK. Efficient & eco-friendly smart nano-pesticides: Emerging prospects for agriculture. Mater Today Proc. 2021;45:3819–24. https://doi.org/10.1016/j.matpr.2021.03.211.
29. Li Y, Li Y, Li Q, Bao J. Rapid biosynthesis of silver nanoparticles based on flocculation and reduction of an exopolysaccharide from *Arthrobacter* sp. B4: its antimicrobial activity and phytotoxicity. J Nanomater. 2017;2017:9703614. https://doi.org/10.1155/2017/9703614.
30. Liu W, Wu Y, Wang C, Li HC, Wang T, Liao CY, Cui L, Zhou QF, Yan B, Jiang GB. Impact of silver nanoparticles on human cells: effect of particle size. Nanotoxicology. 2010;4:319–30. https://doi.org/10.3109/17435390.2010.483745.

31. Mahiuddin M, Saha P, Ochiai B. Green synthesis and catalytic activity of silver nanoparticles based on piper chaba stem extracts. Nanomaterials. 2020;10(9):1777. https://doi.org/10.3390/nano10091777.
32. Malick A, Khodaei N, Benkerroum N, Karboune S. Production of exopolysaccharides by selected *Bacillus* strains: optimization of media composition to maximize the yield and structural characterization. Int J Biol Macromol. 2017;102:539–49. https://doi.org/10.1016/j.ijbiomac.2017.03.151.
33. Mnif I, Ghribi D. Review lipopeptides biosurfactants: mean classes and new insights for industrial, biomedical, and environmental applications. Peptide Sci. 2015;104:129–47. https://doi.org/10.1002/bip.22630.
34. Nicholson WL, Munakata N, Horneck G, Melosh HJ, Setlow P. Resistance of *Bacillus* endospores to extreme terrestrial and extraterrestrial environments. Microbiol Mol Biol Rev. 2000;64:548–72. https://doi.org/10.1128/MMBR.64.3.548-572.2000.
35. Noman M, Ahmed T, Ijaz U, Hameed A, Shahid M, Li D, Song F. Microbe-oriented nanoparticles as phytomedicines for plant health management: an emerging paradigm to achieve global food security. Crit Rev Food Sci Nutr. 2022;7:1–21. https://doi.org/10.1080/10408398.2022.2046543.
36. Noman M, Ahmed T, White JC, Nazir MM, Li D, Song F. *Bacillus altitudinis*-stabilized multifarious copper nanoparticles prevent bacterial fruit blotch in watermelon (*Citrullus lanatus* L.): direct pathogen inhibition, in planta particles accumulation, and host stomatal immunity modulation. Small. 2023;19:e2207136. https://doi.org/10.1002/smll.202207136.
37. Ogunyemi SO, Zhang M, Abdallah Y, Ahmed T, Qiu W, Ali MA, Yan C, Yang Y, Chen J, Li B. The bio-synthesis of three metal oxide nanoparticles (ZnO, MnO2, and MgO) and their antibacterial activity against the bacterial leaf blight pathogen. Front Microbiol. 2020;11: 588326. https://doi.org/10.3389/fmicb.2020.588326.
38. Pinkas D, Fišer R, Kozlík P, Dolejšová T, Hryzáková K, Konopásek I, Mikušová G. *Bacillus subtilis* cardiolipin protects its own membrane against surfactin-induced permeabilization. BBA-Biomembranes. 2020;1862: 183405.
39. Ramey BE, Koutsoudis M, von Bodman SB, Fuqua C. Biofilm formation in plant-microbe associations. Curr Opin Microbiol. 2004;7:602–9. https://doi.org/10.1016/j.mib.2004.10.014.
40. Renzi M, Copini P, Taddei AR, Rossetti A, Gallipoli L, Mazzaglia A, Balestra GM. Bacterial canker on kiwifruit in Italy: anatomical changes in the wood and in the primary infection sites. Phytopathology. 2012;102:827–40. https://doi.org/10.1094/PHYTO-02-12-0019-R.
41. Saha P, Mahiuddin M, Islam ABMN, Ochiai B. Biogenic synthesis and catalytic efficacy of silver nanoparticles based on peel extracts of *Citrus macroptera* fruit. ACS Omega. 2021;6:18260–8. https://doi.org/10.1021/acsomega.1c02149.
42. Saratale RG, Karuppusamy I, Saratale GD, Pugazhendhi A, Kumar G, Park Y, Ghodake GS, Bhargava RN, Banu JR, Shin HS. A comprehensive review on green nanomaterials using biological systems: recent perception and their future applications. Colloids Surf B Biointerfaces. 2018;170:20–35. https://doi.org/10.1016/j.colsurfb.2018.05.045.
43. Servin AD, White JC. Nanotechnology in agriculture: next steps for understanding engineered nanoparticle exposure and risk. NanoImpact. 2016;1:9–12. https://doi.org/10.1016/j.impact.2015.12.002.
44. Shafi J, Tian H, Ji M. *Bacillus* species as versatile weapons for plant pathogens: A review. Biotechnol Biotechnol Equip. 2017;31:446–59. https://doi.org/10.1080/13102818.2017.1286950.
45. Syed B, Prasad N, Dhananjaya BL, Yallappa S, Satish S. Synthesis of silver nanoparticles by endosymbiont *Pseudomonas fluorescens* CA 417 and their bactericidal activity. Enzyme Microb Technol. 2016;95:128–36. https://doi.org/10.1016/j.enzmictec.2016.10.004.
46. Vanaja M, Annadurai G. *Coleus aromaticus* leaf extract mediated synthesis of silver nanoparticles and its bactericidal activity. Appl Nanosci. 2013;3:217–23. https://doi.org/10.1007/s13204-012-0121-9.
47. Wang D, Saleh NB, Byro A, Zepp R, Sahle-Demessie E, Luxton TP, Ho KT, Burgess RM, Flury M, White JC, Su C. Nano-enabled pesticides for sustainable agriculture and global food security. Nat Nanotechnol. 2022;17:347–60. https://doi.org/10.1038/s41565-022-01082-8.
48. Wen L, Zeng P, Zhang L, Huang W, Wang H, Chen G. Symbiosis theory-directed green synthesis of silver nanoparticles and their application in infected wound healing. Int J Nanomed. 2016;11:2757–67. https://doi.org/10.2147/IJN.S106662.
49. Williams RJ, Harrison S, Keller V, Kuenen J, Lofts S, Praetorius A, Svendsen C, Vermeulen L, van Wijnen J. Models for assessing engineered nanomaterial fate and behaviour in the aquatic environment. Curr Opin Environ Sustain. 2019;36:105–15. https://doi.org/10.1016/j.cosust.2018.11.002.
50. Worrall EA, Hamid A, Mody KT, Mitter N, Pappu HR. Nanotechnology for plant disease management. Agronomy. 2018;8:285. https://doi.org/10.3390/agronomy8120285.
51. Xia L, Miao Y, Cao A, Liu Y, Liu Z, Sun X, Xue Y, Xu Z, Xun W, Shen Q, Zhang N, Zhang R. Biosynthetic gene cluster profiling predicts the positive association between antagonism and phylogeny in *Bacillus*. Nat Commun. 2022;13:1023. https://doi.org/10.1038/s41467-022-28668-z.
52. Yu W, Xie H. A review on nanofluids: preparation, stability mechanisms, and applications. J Nanomater. 2012;2012: 435873. https://doi.org/10.1155/2012/435873.
53. Zhang L, Wu L, Si Y, Shu K. Size-dependent cytotoxicity of silver nanoparticles to *Azotobacter vinelandii*: Growth inhibition, cell injury, oxidative stress and internalization. PLoS ONE. 2018;13: e0209020. https://doi.org/10.1371/journal.pone.0209020.

Publisher's Note